Title

Modulation of Mitochondrial Complex I Activity Averts Cognitive Decline in Multiple Animal Models of Familial Alzheimer's Disease

Journal

EBioMedicine, 2(4)

ISSN

2352-3964

Authors

Zhang, Liang
Zhang, Song
Maezawa, Izumi
et al.

Publication Date

2015-04-01

DOI

10.1016/j.ebiom.2015.03.009

Peer reviewed

EBioMedicine 2 (2015) 294–305

Contents lists available at ScienceDirect

EBioMedicine

journal homepage: www.ebiomedicine.com

Original Article

Modulation of Mitochondrial Complex I Activity Averts Cognitive Decline in Multiple Animal Models of Familial Alzheimer's Disease

Liang Zhang [a], Song Zhang [b], Izumi Maezawa [c,d], Sergey Trushin [a], Paras Minhas [a], Matthew Pinto [a], Lee-Way Jin [c,d], Keshar Prasain [e], Thi D.T. Nguyen [e], Yu Yamazaki [f], Takahisa Kanekiyo [f], Guojun Bu [f], Benjamin Gateno [a], Kyeong-Ok Chang [g], Karl A. Nath [h], Emirhan Nemutlu [i], Petras Dzeja [b], Yuan-Ping Pang [j], Duy H. Hua [e], Eugenia Trushina [a,j,*]

[a] Department of Neurology, Mayo Clinic, Rochester, MN 55905, USA
[b] Division of Cardiovascular Research, Mayo Clinic, Rochester, MN 55905, USA
[c] MIND Institute, University of California Davis, Sacramento, CA 95814, USA
[d] Department of Pathology, University of California Davis, Sacramento, CA 95814, USA
[e] Department of Chemistry, CBC Building, Kansas State University, Manhattan, KS 66506, USA
[f] Department of Neuroscience, Mayo Clinic, Jacksonville, FL 32224, USA
[g] Department of Diagnostic Medicine Pathobiology, College of Veterinary Medicine, Kansas State University, Manhattan, KS 66506, USA
[h] Department of Nephrology, Mayo Clinic, Rochester, MN 55905, USA
[i] Hacettepe University, Faculty of Pharmacy, Department of Analytical Chemistry, Sihhiye, Ankara 06100, Turkey
[j] Department of Molecular Pharmacology and Experimental Therapeutics, Mayo Clinic, Rochester, MN 55905, USA

ARTICLE INFO

Article history:
Received 20 January 2015
Received in revised form 6 March 2015
Accepted 10 March 2015
Available online 12 March 2015

Keywords:
Mitochondrial complex I activity
Cellular energetics
Alzheimer's disease
AMPK
Amyloid beta
Hyperphosphorylated tau
GSK3beta
Axonal trafficking
Animal models of familial AD

ABSTRACT

Development of therapeutic strategies to prevent Alzheimer's disease (AD) is of great importance. We show that mild inhibition of mitochondrial complex I with small molecule CP2 reduces levels of amyloid beta and phospho-Tau and averts cognitive decline in three animal models of familial AD. Low-mass molecular dynamics simulations and biochemical studies confirmed that CP2 competes with flavin mononucleotide for binding to the redox center of complex I leading to elevated AMP/ATP ratio and activation of AMP-activated protein kinase in neurons and mouse brain without inducing oxidative damage or inflammation. Furthermore, modulation of complex I activity augmented mitochondrial bioenergetics increasing coupling efficiency of respiratory chain and neuronal resistance to stress. Concomitant reduction of glycogen synthase kinase 3β activity and restoration of axonal trafficking resulted in elevated levels of neurotrophic factors and synaptic proteins in adult AD mice. Our results suggest that metabolic reprogramming induced by modulation of mitochondrial complex I activity represents promising therapeutic strategy for AD.

1. Introduction

Alzheimer's disease (AD) is a devastating neurodegenerative disorder without cure. It is associated with progressive cognitive decline that affects aging population. Without effective and immediate approaches aimed to prevent or modify the disease, by 2050 the number of affected individuals can reach 100 million (Thies et al., 2013). Extracellular amyloid beta (Aβ) plaques and intracellular neurofibrillary tangles comprised of hyperphosphorylated Tau protein (pTau) represent the major hallmarks of AD (Braak and Braak, 1991). The etiology of sporadic AD, which represents over 95% of all cases, is unknown with age being the single risk factor. Familial AD (FAD) is caused by mutations in presenilin 1 and presenilin 2 (PS1 and PS2), and amyloid precursor protein (APP), all of which are involved in the abnormal processing of APP leading to increased levels of Aβ (Holtzman et al., 2011). The specific molecular mechanisms of sporadic and familial AD are still under investigation hindering the development of effective therapeutic approaches. There is compelling data to demonstrate that increased levels of Aβ compromise multiple cellular pathways. Thus, the downstream cognitive symptoms can be caused by non-Aβ factors including oxidative stress, inflammation, mitochondrial dysfunction, and lipid perturbations (Pimplikar et al., 2010). At the same time, emerging data from multiple animal studies and clinical investigations suggest a tight interconnection between Aβ and pTau, and therefore, development of strategies to reduce levels of both could be beneficial (Jack and Holtzman, 2013; Mondragon-Rodriguez et al., 2012).

* Corresponding author at: Department of Neurology, Mayo Clinic, 200 First St. SW, Rochester, MN 55905, USA.
E-mail address: Trushina.Eugenia@mayo.edu (E. Trushina).

http://dx.doi.org/10.1016/j.ebiom.2015.03.009

However, to date, all clinical trials designed to low levels of Aβ by either blocking activity of β or γ secretases, preventing Aβ aggregation, or promoting Aβ clearance by immunotherapy have failed (Cummings et al., 2014) emphasizing an urgent need to find new therapies for AD. One of the emerging therapeutic approaches involves modulation of cellular energetics that includes activation of AMP-activated protein kinase (AMPK), a master regulator of intracellular energy metabolism (Shirwany and Zou, 2014). AMPK activation was shown to promote neuronal survival after the exposure to Aβ peptides, induce autophagy-dependent degradation of Aβ, and reduce tau phosphorylation (Park et al., 2012; Salminen et al., 2011; Vingtdeux et al., 2010, 2011). Resveratrol-induced activation of AMPK reduced cognitive impairment in SAMP8 mouse model of AD (Porquet et al., 2013). AMPK activation is also linked to an increase in life span in model organisms (Kenyon, 2010; Mair et al., 2011; Salminen and Kaarniranta, 2012), and to prevention of obesity and insulin resistance, conditions that significantly and independently increase risk of AD (Hardie, 2007; Profenno et al., 2010). Metformin, an FDA approved drug to treat type 2 diabetes and potent activator of AMPK (Pernicova and Korbonits, 2014), reduces tau phosphorylation and improves neuronal insulin signaling and AD-related neuropathological changes in vitro (Gupta et al., 2011; Kickstein et al., 2010). However, activation of AMPK has been shown to contribute to AD pathology and cause brain damage in AD mice (Cai et al., 2012; Mairet-Coello et al., 2013). Similar, metformin was also shown to increase Aβ levels by up-regulating the activity of beta-site APP-cleaving enzyme 1 (BACE1), which could account for increased risk of AD development in diabetic patients treated with metformin (Imfeld et al., 2012; Moore et al., 2013). Thus, the development of safe metabolic modulators for AD treatment represents a considerable challenge.

Previously, we have synthesized several tricyclic pyrone compounds based on the structures of pyripyropene A, a potent acyl-CoA:cholesterol O-acyltransferase inhibitor (Omura et al., 1993), and arisugacin, a potent acetylcholinesterase inhibitor (Hua et al., 1997; Omura et al., 1995). One of the compounds, CP2, was found to attenuate Aβ-induced toxicity in primary cortical neurons (Maezawa et al., 2006) and reduce Aβ aggregation in 5× transgenic animal model of familial AD (Hong et al., 2009). Here, we report that mild inhibition of mitochondrial complex I with tricyclic pyrone compound CP2 reduces levels of both Aβ and pTau and averts the development of cognitive and behavior phenotype in three mouse models of FAD. We identified CP2 binding site in the redox center of complex I, and defined the molecular mechanism that involves activation of AMPK and restoration of axonal trafficking. Our results provide compelling evidence that modulation of complex I activity represent promising and alternative therapeutic strategy for AD.

2. Material and Methods

2.1. Chemicals

CP2 was synthesized as described by Hua et al. (2003) and purified using HPLC.

2.2. Animals

Animal care and handling procedures were approved by the Mayo Clinical Institutional Animal Care and Use Committee in accordance with the National Institutes of Health's *Guide for the Care and Use of Laboratory Animals*. Details utilized animal models, treatment regimens and behavior and memory tests are presented in Supplemental Experimental Procedures.

2.3. Gene Expression

Hippocampal tissue from untreated and CP2-treated (4 months) APP/PS1 (n = 5) and NTG (n = 5) mice was examined for the markers of inflammation (iNOS, RANTES and interferon-gamma), cholesterol efflux (ABCA1 and ABCG1) and housekeeping gene (β-actin). Total RNA was extracted with RNeasy kit (Qiagen). Gene expression assay (real time qPCR) was performed with the primers/probe kit (Applied Biosystem Inc.) according to the manufacturer's protocol. The expression levels of each gene from each group of animals were calculated as per cent of the expression relative to the control NTG animals after normalization for β-actin. Experiments were repeated twice in two independent cohorts.

2.4. Neuronal Cultures

Primary hippocampal and cortical neurons were cultured as described by Trushina et al. (2012). Neurons from neonatal animals (P1) were isolated and plated from individual pups; genotyping was done prior to the day of experiment. All experiments were performed in neurons 7 days in culture unless specifically stated. Details are described in Supplemental Experimental Procedures.

2.5. CP2 Quantification

Animals were euthanized via cervical dislocation. Organs were harvested on ice and immediately flash frozen in liquid nitrogen. On the day of analysis, tissue was homogenized, and CP2 was extracted with a mixture of ethyl acetate and 1-propanol (9:1), and analyzed using LC/MS/MS mass spectrometer. Benzenetetracarboxylic acid (BTA) was used as an internal standard (see Supplemental Experimental Procedures for details).

2.6. Brain Amyloid

Amyloid plaques were visualized using immunofluorescence labeling and confocal microscopy as previously described (Maezawa et al., 2004). Three brain slices were examined from each mouse. Average particle size of the plaques was quantified using Image J 1.45 (rsbweb.nih.gov/ij/) (see Supplemental Experimental Procedures for details).

2.7. Aβ ELISA

Soluble Aβ levels were determined in brain tissue isolated from CP2-treated APP/PS1 mice 7 months old (Kanekiyo et al., 2013). Details are presented in Supplemental Experimental Procedures.

2.8. Axonal Trafficking

Imaging of mitochondrial trafficking in live cortical neurons and data analysis was done as described by Trushina et al. (2004, 2012). Details are described in Supplemental Experimental Procedures.

2.9. Subcellular Fractionation and CP2 Localization

Cortical neurons and brain tissue from animals treated with CP2 for 4 months were homogenized, and subcellular fractionation was done using differential centrifugation as described by Okado-Matsumoto and Fridovich (2001). Concentration of CP2 in cellular fractions was determined using LC/MS/MS as described above.

2.10. Mitochondrial Respiration

Mitochondrial respiration and rate of glycolysis was determined in cortical neurons (E17) isolated from WT mice using an XF24 Extracellular Flux Analyzer (Seahorse Biosciences, North Billerica, MA, USA) as described by Wu et al. (2007). Details of experiment are described in Supplemental Experimental Procedures.

2.11. ATP, ADP, and AMP Levels

ATP, ADP and AMP levels in neurons and brain tissue were estimated using HPLC. Details of experiment are described in Supplemental Experimental Procedures.

2.12. Citrate Synthase Assay

The citrate synthase activity was determined in brain tissue of CP2-treated and untreated WT and APP/PS1 mice ($n = 5$ per each group) according to the manufacturer's instructions (Sigma-Aldrich, Co.).

2.13. Activity of Complexes I–V

Complex I–V enzymatic activity was measured photometrically (Spinazzi et al., 2012). Details of experiment are described in Supplemental Experimental Procedures.

2.14. NAD^+/NADH Levels

WT cortical neurons were treated with vehicle (0.001% DMSO) or different concentrations of CP2 for 24 h before NAD^+/NADH levels were determined using Luminescence assay (Promega) according to the manufacturer's instructions.

2.15. H_2O_2 Treatment

WT cortical neurons were pre-treated with different concentrations of CP2 for 24 h, after that 1 mM H_2O_2 was added for 2 h. Cell viability was determined using CellTiter-Glo® Luminescent Cell Viability Assay (Promega) according to the manufacturer's instructions.

2.16. Transmission Electron Microscopy

EM images of hippocampal brain tissue from FAD mice were obtained as described by Trushina et al. (2012).

2.17. Western Blotting

Western blotting was conducted as described (Trushina et al., 2012); see Supplemental Experimental Procedures for details.

2.18. Theoretical Model of the CP2-Bound FMN Subunit of Human Mitochondrial Complex I

For details on low-mass molecular dynamics simulations see Supplemental Experimental Procedures.

2.19. Data Analysis

Statistical analyses of means for more than two groups were performed using one-way analysis of variance (ANOVA) with the categories of genotype and age as independent factors followed by the Newman–Keuls post-hoc test for multiple comparisons. For analyses of means involving only two groups with a sample size $n < 30$, the F-test was used to determine if the variances between the two groups were significantly different. For samples with a significant difference in variance, the Welch's *t* test was applied. Two-tailed *t*-test was applied for the samples with an insignificant difference in variance or where $n \geq 30$. The null hypothesis was rejected at the 0.05 level. All statistical computations were carried out using Prism (Graphpad Software). Axonal trafficking videos were manually analyzed using LSM Image Browser (version 4.2, Zeiss Microimaging, Thornwood, New York, USA) (Trushina et al., 2012). Unpaired *t*-test with Welch's correction was used for analyzing axonal trafficking data. In all cases, $\alpha = 0.05$ was considered significant. All values are presented as mean ± standard error.

3. Results

3.1. CP2 Averts Cognitive and Behavior Phenotype in FAD Mice

We have previously identified small molecule tricyclic pyrone CP2 (Fig. 1A) that protects cells against Aβ toxicity, and reduces brain Aβ in 5× FAD mice (Hong et al., 2009; Maezawa et al., 2006). To examine the molecular mechanism, we first tested whether CP2 penetrates the blood–brain barrier (BBB). C^{14}-Labeled CP2 was injected intraperitoneally to wild type (WT) mice, and levels were measured in the brain tissue 30 min post-injection (Fig. S1A, B). Results suggest that CP2 rapidly accumulates in the brain. Additional pharmacokinetics studies conducted in plasma of WT mice after intravenous or oral administration demonstrated that CP2 bioavailability is 43% (Fig. S1C, D).

To examine the effect of CP2 administration on the development of behavior and memory phenotype in vivo, breeding heterozygous APP and PS1 mice were treated with 25 mg/kg/day CP2 in drinking water and progeny with all four genotypes were produced with the expected ratio (Fig. 1B). F1 animals continued to receive CP2 through life till 14 months of age. F1 APP and PS1 heterozygous mice also produced multiple litters (Fig. 1B, F2). CP2-treated P and F1 mice were well groomed, displayed no physical differences compared to non-transgenic (NTG) littermates, with fecundity prolonged up to 14 months of age, while untreated counterparts were heavier and stopped producing progeny earlier in life (Figs. 1C, D and S2). Histopathological examination of newborn F2 mice treated in utero and F1 mice treated through life (Fig. 1B) demonstrated lack of developmental or other abnormalities. Average concentration of CP2 in the brain of newborn mice was ~90 μM, and in adult mice ~130 μM, regardless of the duration of treatment (Table S1). Highest concentrations were found in brain, heart, and reproductive organs, while levels in the liver were the lowest (Table S2).

The effect of chronic CP2 treatment starting in utero on the development of memory and behavior phenotype was determined with a battery of techniques. CP2-treated 56-weeks old APP and PS1 mice performed significantly better on hanging bar and on the rotating rod (Fig. 1E, F) compared to NTG mice and untreated counterparts. Results of novel object recognition (NOR) test confirmed the development of progressive memory deficit in untreated PS1 and APP mice starting at 30 weeks of age (Fig. 1G, H). In contrast, CP2-treated FAD mice did not demonstrate cognitive impairment at any age tested (Fig. 1G, H).

We next investigated whether CP2 administered to adult presymptomatic mice delayed the onset of the disease. Double transgenic APP/PS1 mice have accelerated AD phenotype with amyloid deposition and altered behavior in Y-maze present at 3 months of age (Holcomb et al., 1998). APP/PS1 mice treated with CP2 starting at 2.5 months of age (Fig. 2A) outperformed their untreated counterparts in the hanging bar test and maneuvering on accelerating rod evident after 4 months of treatment (Fig. 2B, C), and did not develop anxiety in the open field test (Fig. 2D). Similar to APP and PS1 mice, CP2 treatment averted the development of cognitive decline in APP/PS1 animals preserving the ability to discriminate between novel and familiar objects (Fig. 2E). Memory protection was detected after 2 months of treatment. In the T-maze, CP2-treated APP/PS1 mice displayed higher percentage of spontaneous alternations compared to NTG or untreated APP/PS1 animals, indicating a superior working memory and intact exploratory behavior (Fig. 2F).

3.2. CP2 Treatment Reduces Soluble and Insoluble Aβ

Levels of amyloid beta in the brain tissue of CP2-treated and untreated FAD mice were established using confocal microscopy (Maezawa et al., 2004). We found that treatment for 4 months starting at presymptomatic age of 2.5 months (Fig. 2A) resulted in a 50% reduction in

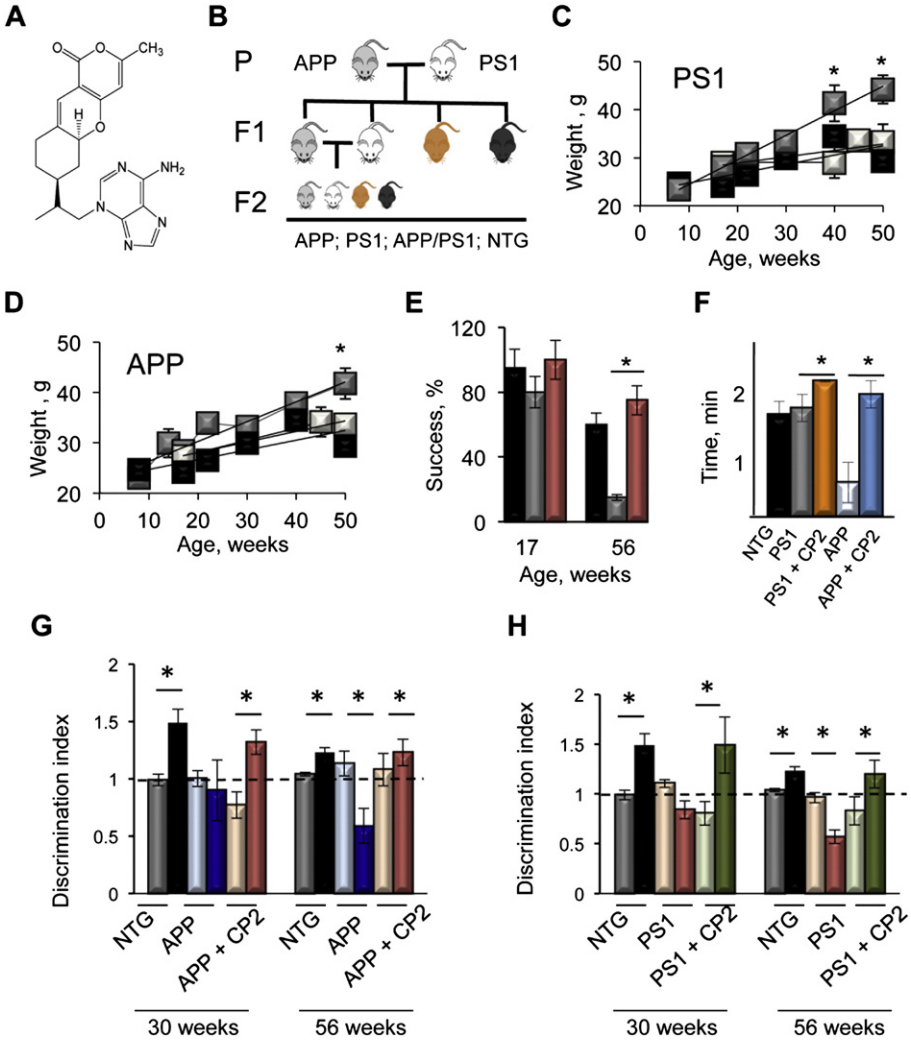

Fig. 1. Chronic CP2 treatment averts the development of behavior and memory phenotype in FAD mice. (A) CP2 structure. (B) P and F1 animals treated with 25 mg/kg/day CP2 produced F1 progeny that were treated with CP2 till 14 months of age. F2 pups were used for axonal trafficking experiments. (C, D) CP2-treated PS1 (C, light gray; n = 5) and APP (D, light gray, n = 5) mice maintained body weight similar to NTG untreated mice (black, n = 10), while untreated PS1 (C, dark gray, n = 10) and APP (D, dark gray, n = 10) mice accumulated weight with age. $^*P < 0.05$. (E) CP2-treated APP mice (red, n = 5) did not display muscle weakness or altered prehensile reflex in hanging bar test compared to untreated APP animals (gray, n = 10). Black — untreated NTG, n = 10. $^*P < 0.05$. (F) Time on a rod rotating at 20 rpm. CP2-treated PS1 (orange, n = 5) and APP (dark blue, n = 5); untreated APP (light blue, n = 10), PS1 (gray, n = 10), and NTG mice (black, n = 10). Mice were 56 weeks old. $^*P < 0.05$. (G, H) NOR test demonstrates that CP2-treated APP (G, light orange bars: training session; red bars: NOR, n = 5) and PS1 (H, light blue bars: training session; dark blue bars: NOR, n = 5) mice maintained the ability to recognize a familiar object similar to NTG animals (n = 10) while their untreated counterparts (n = 10 for APP and n = 10 for PS1) lost that ability with age. $^*P < 0.05$. See also Figs. S1 and S2.

plaques compared to age- and sex-matched untreated APP/PS1 mice similar to our previous results in 5× FAD mice (Hong et al., 2009) (Figs. 3A and S3). CP2-treated APP/PS1 mice also had a significant decrease in the levels of soluble Aβ42 detected using ELISA (Fig. 3B, C). These data suggest that cognitive protection induced by CP2 is accompanied with significant decrease in brain Aβ.

3.3. Modulation of Complex I Activity Augments Mitochondrial Bioenergetics

We next assessed CP2 localization in cortical neurons and brain tissue of WT and APP/PS1 mice. Subcellular fractionation and HPLC analysis revealed that CP2 accumulated in enriched mitochondrial fractions isolated from CP2-treated neurons in vitro (Fig. 3D, E). Similar, CP2 predominantly was detected in enriched mitochondrial fractions isolated from different brain regions of CP2-treated WT and APP/PS1 mice (Fig. S4). Notably, CP2 levels were highest in the mitochondrial fractions from the hippocampus of both WT and APP/PS1 mice compared to other brain regions or nuclear or cytoplasmic fractions. Overall CP2 levels were higher in all fractions in APP/PS1 mice compared to WT animals consistent with its reported ability to bind Aβ (Hong et al., 2009).

To evaluate whether CP2 affects mitochondrial bioenergetics, we simultaneously measured oxygen consumption rate (OCR) and glycolysis (ECAR, extracellular acidification rate) in intact WT cortical neurons using a Seahorse XF24 extracellular flux analyzer (Figs. 4 and S5A, B). We found that CP2-treated neurons exhibited significantly lower basal OCR relative to the vehicle-treated cells (Fig. 4A, B). We next investigated whether CP2 affected individual components of electron transport chain (ETC) by adding specific pharmacological inhibitors to CP2-treated and untreated cells and measuring OCR (Fig. 4A, B). A decrease in OCR after the addition of the Complex V inhibitor oligomycin was compatible in treated and untreated neurons indicating that CP2 did not affect ATP synthase (Fig. S5B). However, we found that CP2 significantly augmented spare respiratory capacity (SRC) evident as an increase in OCR in response to the addition of mitochondria uncoupler FCCP (Figs. 4A, B and S5B). SRC is an indicator of the mitochondrial ability to produce additional energy under conditions of increased workload or stress, which is essential for long-term cellular survival and

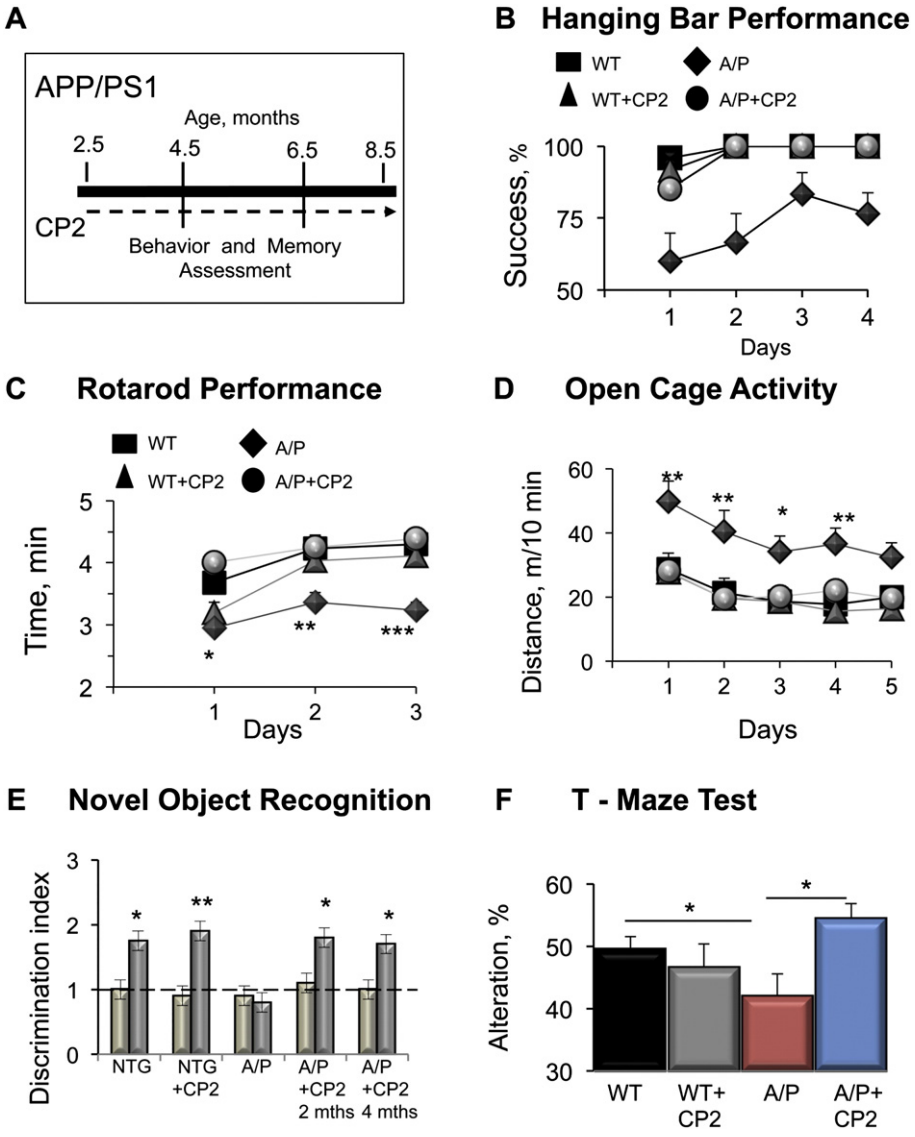

Fig. 2. CP2 treatment of pre-symptomatic APP/PS1 mice prevents the development of AD. (A) Treatment regimen in pre-symptomatic APP/PS1 (A/P) mice. (B, C) CP2 protects against the development of motor phenotype evident by the unaltered performance on a hanging bar (B) and accelerating rod (C) after 4 months of treatment. Squares — WT; triangles — WT + CP2; diamonds — A/P; circles — A/P + CP2. $^{*}P < 0.05$; $^{**}P < 0.01$; $^{***}P < 0.001$; n = 8–9 mice per group. (D) A/P mice (circles) treated for 4 months demonstrated normal activity in the cage similar to untreated (squares) and CP2-treated (triangles) WT mice compared to the untreated A/P animals (diamonds). $^{*}P < 0.05$; $^{**}P < 0.01$ A/P compared to WT; $^{\#\#}P < 0.01$ A/P + CP2 compared to A/P; n = 8–9 mice per group. (E) NOR test. $^{*}P < 0.05$; $^{**}P < 0.01$; n = 5–10 mice per group. (F) After 4 months of treatment, A/P mice performed similar to WT animals during spontaneous T-maze exploration while untreated A/P mice displayed prominent memory deficit. $^{*}P < 0.05$. Data are presented as mean ± SEM.

function (Choi et al., 2009). Similarly, CP2 increased mitochondrial state apparent (Fig. 4D) and respiratory control ratio (Fig. 4E), and reduced proton leak (Fig. 4B), which together suggest that ETC in neurons was tightly coupled (Fig. 4C) providing mitochondria with a considerable bioenergetics reserve and enhanced ability to sustain stress. Indeed, CP2-treated neurons exhibited significantly greater resistance to H_2O_2-induced oxidative damage compared to untreated neurons (Fig. 4F). Reduced respiration could lead to the upregulation of glycolytic pathway. However, the decrease in OCR in response to oligomycin in CP2-treated neurons did not increase ECAR (Fig. 4G) indicating lack of shift to glycolysis. Thus, CP2 reduces mitochondrial respiration and augments bioenergetics without activating glycolytic pathway.

To further investigate the mechanism of CP2-induced reduction in basal OCR, we substituted specific inhibitors of ETC and FCCP with CP2, one at a time, and evaluated whether CP2 prompts changes in OCR similar to any of the mitochondrial toxicants (Fig. 4H). Addition of CP2 to intact WT neurons induced changes similar to rotenone/antimycin A but not oligomycin or FCCP suggesting that CP2 inhibits complexes I and/or III (Fig. 4H). To confirm these findings, we examined the effect of CP2 on the activity of each of the respiratory complexes using enzymatic assays and mitochondria isolated from the brain of WT mice (Fig. 5A). The addition of CP2 did not alter the activity of complexes II, III, IV and V, while complex I activity was inhibited in a dose-dependent manner. However, the effect was mild compared to 80% of inhibition induced under the same experimental conditions by 10 μM of rotenone (data not shown). It is well known that inhibition of complex I could increase production of reactive oxygen species (ROS) contributing to neurodegenerative processes (Dumont and Beal, 2011). Nevertheless, the expression of oxidant-inducible gene, heme oxygenase-1 (HO-1) (Nath et al., 2001), or genes related to inflammation (iNOS, RANTES and interferon-gamma, IFNγ) was not affected in the brain tissue of FAD mice after 4 or 14 months of CP2 treatment (Figs. 5B, C and S6). Moreover, there appears a trend toward a reduction in expression of HO-I, iNOS, IFNγ in hippocampus of CP2-treated FAD animals. We previously reported that CP2 modestly inhibited the activity of Acyl-CoA:cholesterol acyltransferase, which could increase the

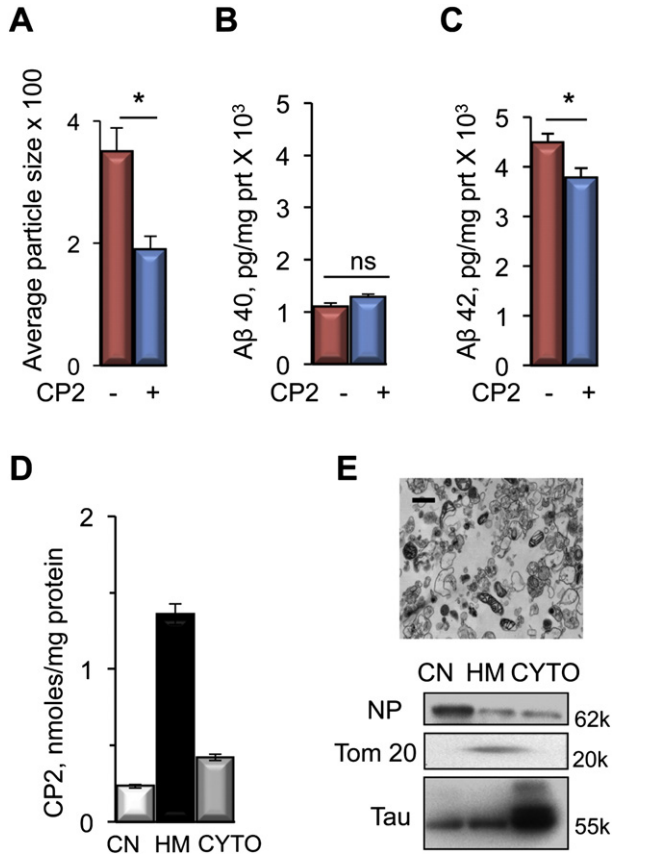

Fig. 3. CP2 reduces amyloid levels and accumulates in mitochondria. (A) Amyloid plaques in the brain of APP/PS1 mice (blue, n = 5) treated for 4 months are significantly reduced compared to untreated animals (red, n = 5). *$P < 0.05$. (B, C) Soluble Aβ42 (C) but not Aβ40 (B) is reduced in APP/PS1 mice treated for 6 months (blue, n = 9) compared to untreated animals (red, n = 9). *$P < 0.05$. (D) CP2 accumulates in mitochondria (HM) fractions isolated from WT neurons treated with 2 μM CP2 for 24 h. CN — crude nuclear; CYTO — cytoplasmic fractions. (E) Purity of HM fractions confirmed using EM (scale bar, 1 μm) and Western blotting. Tom 20 — mitochondrial marker; NP — nucleoporin. See also Figs. S3 and S4.

expression of cholesterol transporter genes (Pokhrel et al., 2012). However, gene expression analysis failed to detect activation of cholesterol transporter genes ABCA1 or ABCG1 suggesting that therapeutic effect of CP2 was not related to enhanced cholesterol efflux (Fig. S6). We next assayed the activity of citrate synthase, an enzyme of the mitochondrial matrix that is a marker of organelle integrity and oxidative capacity. Citrate synthase activity in mitochondria isolated from brain tissue of CP2-treated APP/PS1 mice was similar to the observed in WT animals (Fig. S5C) suggesting that CP2 does not damage inner mitochondrial membrane causing leakage of the matrix and does not affect oxidative capacity or TCA cycle. These results are also supported by electron microscopy examination demonstrating robust mitochondrial morphology and cristae organization in the hippocampus of APP, PS1 and APP/PS1 mice treated with CP2 through life (Fig. 5D).

Furthermore, low-mass molecular dynamics simulations (Pang, 2014) suggest that the cationic CP2 molecule competes with flavin mononucleotide (FMN) for binding to the redox subunit of human mitochondrial complex I (Fig. 5E, F). FMN is involved in the oxidation of nicotinamide adenine dinucleotide NADH to NAD^+ (Hirst et al., 2003). Indeed, treatment of WT neurons with CP2 increased levels of NADH in a dose-dependent manner compared to vehicle or an inactive CP2 analog, a neutral tricyclic pyrone compound TP17 (Hong et al., 2009) (Fig. 5G). However, inhibition of complex I by CP2 did not lead to a significant drop in the cellular NAD^+ concentration (Fig. 5G). These computational and biochemistry studies indicate that competition for binding at the FMN subunit partially reduces complex I activity without inducing oxidative damage or inflammation in vivo.

3.4. Modulation of Complex I Activates AMPK In Vitro and In Vivo

We next measured ATP, AMP and ADP in vitro in primary neurons and in brain tissue of CP2-treated animals (Fig. 6A–G). Modulation of complex I activity resulted in reduced ATP levels in neurons and dose- and time-dependent increase in AMP/ATP and a decrease in ATP/ADP ratio (Fig. 6A–D) consistent with previously shown decrease in mitochondrial respiration (Fig. 4A, B). Similarly, reduced ATP, increased AMP levels and AMP/ATP ratio was detected in the brain tissue of CP2-treated WT and APP/PS1 mice (Fig. 6E–G). Increase in AMP/ATP is a known activator of AMPK, a major energy sensor in the cell (Shirwany and Zou, 2014). Indeed, CP2 treatment increased levels of pAMPK (Thr172), an activated form of the kinase, in neurons from APP/PS1 mice in time-dependent manner (Figs. 6H and S7A), and in the brain tissue of WT and APP/PS1 animals in vivo (Figs. 6I and S7B). AMPK negatively regulates the activity of glycogen synthase kinase 3 beta (GSK3β), which in turn could affect tau phosphorylation (Horike et al., 2008; Park et al., 2012). Indeed, CP2-dependent activation of AMPK resulted in concomitant increase in the inhibitory phosphorylation of GSK3β at Ser9 and marked reduction of tau phosphorylation at Ser396/404 in neurons in vitro and in APP/PS1 mice in vivo (Fig. 6H, I).

3.5. CP2 Restores Axonal Trafficking

We previously reported that inhibition of axonal trafficking was detected early in embryonic neurons from PS1 and APP/PS1 mice (Trushina et al., 2012). Increased levels of Aβ, pTau and activated GSK3β are implicated in the development of axonal trafficking dysfunction in AD (Vicario-Orri et al., 2015). We next explored whether changes induced by modulation of complex I activity positively affected axonal transport. Using established methodology (Trushina et al., 2004, 2012) (Fig. 7A–C), we evaluated mitochondrial motility in neurons from F2 pups treated with CP2 in utero (Fig. 1B). Visualization of mitochondrial dynamics in live neurons revealed lack of trafficking inhibition in APP/PS1 and PS1 mice in both anterograde and retrograde directions (Fig. 7B–D) and significant increase in motile organelles (Fig. 7E). Since CP2 levels were similar in the brain tissue of neonatal F2 and adult FAD animals (Table S1, P1), we examined whether axonal trafficking was also improved in adult mice in vivo by measuring levels of brain-derived neurotrophic factor (BDNF) in APP/PS1 mice treated with CP2 for 2 months (Fig. 7F). BDNF provides an essential support for synaptic function, plasticity and neuronal survival. It is delivered to the cell body via retrograde trafficking, and its reduced availability is among the most devastating consequences of axonal trafficking inhibition (Poon et al., 2011). Restoration of axonal transport and improved BDNF support could positively affect levels of synaptic proteins. Indeed, we found significant increase in synaptophysin and BDNF in brain tissue of CP2-treated APP/PS1 mice (Fig. 7F–I) consistent with preserved cognitive function.

4. Discussion

We present evidence that modulation of cellular energetics via mild inhibition of mitochondrial complex I reduces levels of both Aβ and pTau and averts the development of cognitive phenotype in multiple FAD mice. Using low-mass molecular dynamics simulations and multiple biochemical approaches, we identified that CP2 competes with FMN for binding to the redox center of human mitochondrial complex I. We conducted comprehensive animal studies utilizing three distinct, transgenic mouse models of FAD with early and late disease onset and two treatment regimens that demonstrate unequivocal protection of mice against cognitive decline as well as enhanced vigor and fecundity relative to untreated groups. We also performed in-depth evaluation

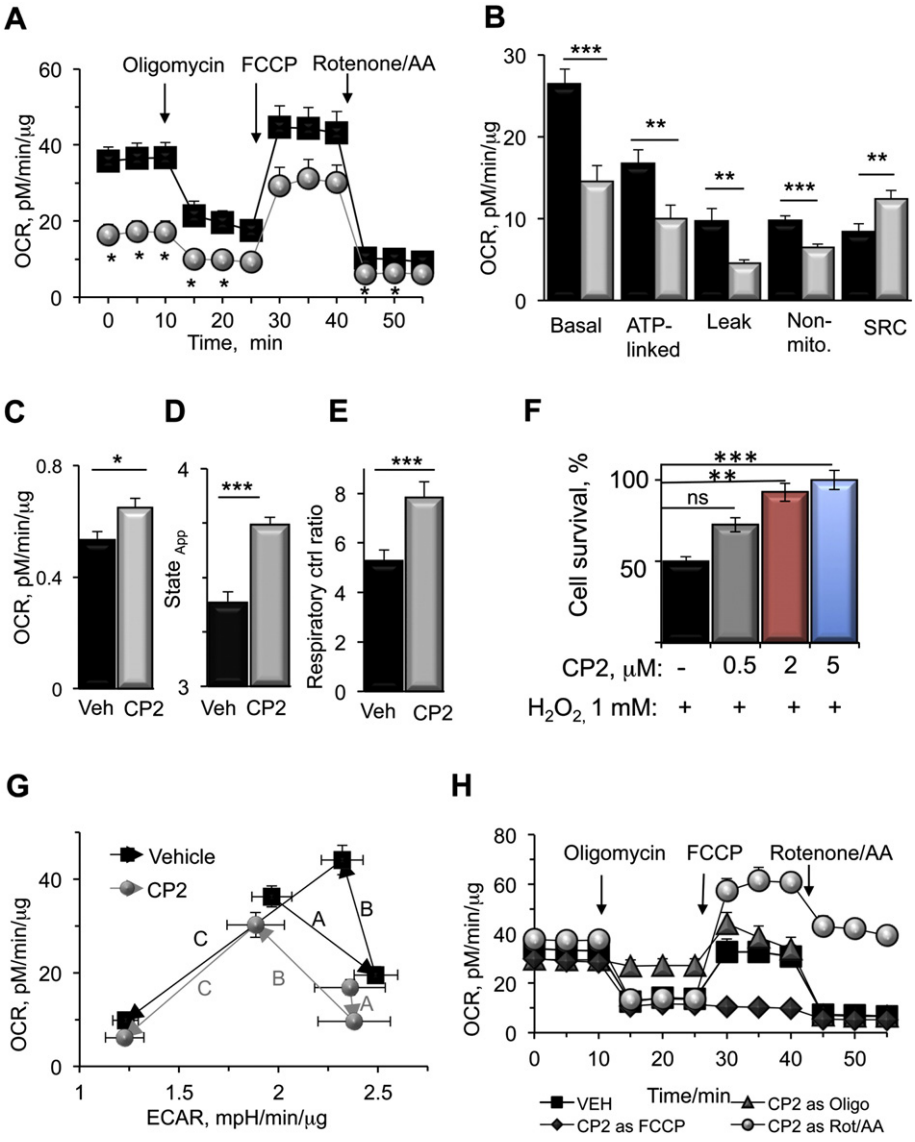

Fig. 4. CP2 augments mitochondrial bioenergetics in neurons. (A–E) Bioenergetics parameters estimated in WT cortical neurons treated with 2 μM CP2 (24 h, gray) compared to vehicle-treated neurons (black). Data are mean ± SEM; n = 12–14 replicates per data point, three independent experiments. OCR — oxygen consumption rate; SRC — spare respiratory capacity; non-mito — non-mitochondrial respiration; AA — antimycin A. Coupling efficiency is presented in (C). $^{*}P < 0.05$; $^{**}P < 0.01$; $^{***}P < 0.001$ (Student's *t*-test). (F) CP2 protects WT neurons against H_2O_2 toxicity. $^{**}P < 0.01$; $^{***}P < 0.001$ (Student's *t* test). (G) CP2 treatment does not induce glycolysis. Temporal bioenergetic profiling in neurons generated as in (A) after addition of: A — oligomycin, B — FCCP, and C — rotenone (n = 12–14 replicates per data point, three independent experiments). (H) CP2 mimics the effect of rotenone/AA; n = 7. See also Fig. S5.

of molecular mechanisms in vitro and in vivo determining that changes in cellular energetics led to an increase in AMP/ATP ratio and activation of AMPK, with subsequent reduction in GSK3β and restoration of axonal trafficking (Fig. 7J). Our findings demonstrate that modulation of mitochondrial function by small-molecule therapeutics could effectively and safely modify or prevent the development of disease validating promising and alternative therapeutic strategy for AD that may offer a practical treatment to patients.

Complex I is the largest and most complicated enzyme of the mammalian OXPHOS system where function of its 45 subunits is not entirely understood. Deficiencies in complex I are associated with various diseases including Parkinson's disease, Huntington's disease (HD) and AD (Orth and Schapira, 2001). Complex I is also one of the main contributors to ROS production (Hirst et al., 2008). However, CP2-dependent inhibition of complex I did not induce oxidative damage, inflammation or changes in mitochondrial morphology. Contrary, CP2 augmented mitochondrial bioenergetics increasing SRC and ETC coupling efficiency, conferring neurons with greater ability to resist stress. Chronic treatment for 14 months provided robust preservation of cognitive and motor functions in FAD animals compared not only to untreated counterparts but also to WT mice. The beneficial metabolic adaptation observed in our study may be related to the specific site of CP2 binding to complex I that is encoded by the NADH-ubiquinone oxidoreductase 1 alpha subcomplex subunit 1 (NDUFA1). It is interesting to note that partial deficiency induced by neuron-specific conditional ablation of another subunit of complex I, NDUFA5, also did not increase oxidative damage or inflammation, but contrary to our data, caused mild chronic encephalopathy in mice (Peralta et al., 2014). Moreover, different from rotenone that binds at or close to the ubiquinone binding site(s) of complex I leading to substantial ROS generation (Darrouzet et al., 1998), binding at the FMN subunit can actually reduce levels of ROS by inhibiting the reaction of semiquinone species with O_2 that occurs at the flavin center (King et al., 2009). It is also important to note that the extent of complex I inhibition by CP2 was mild. Thus, it did not significantly affect the pool of NAD^+. At the same time, it is feasible that moderate shift of the equilibrium toward NADH detected in our studies could have an additional benefit compensating for a decline in its neuronal levels associated with age and AD (Parihar and Brewer, 2007). Moreover, since inhibition

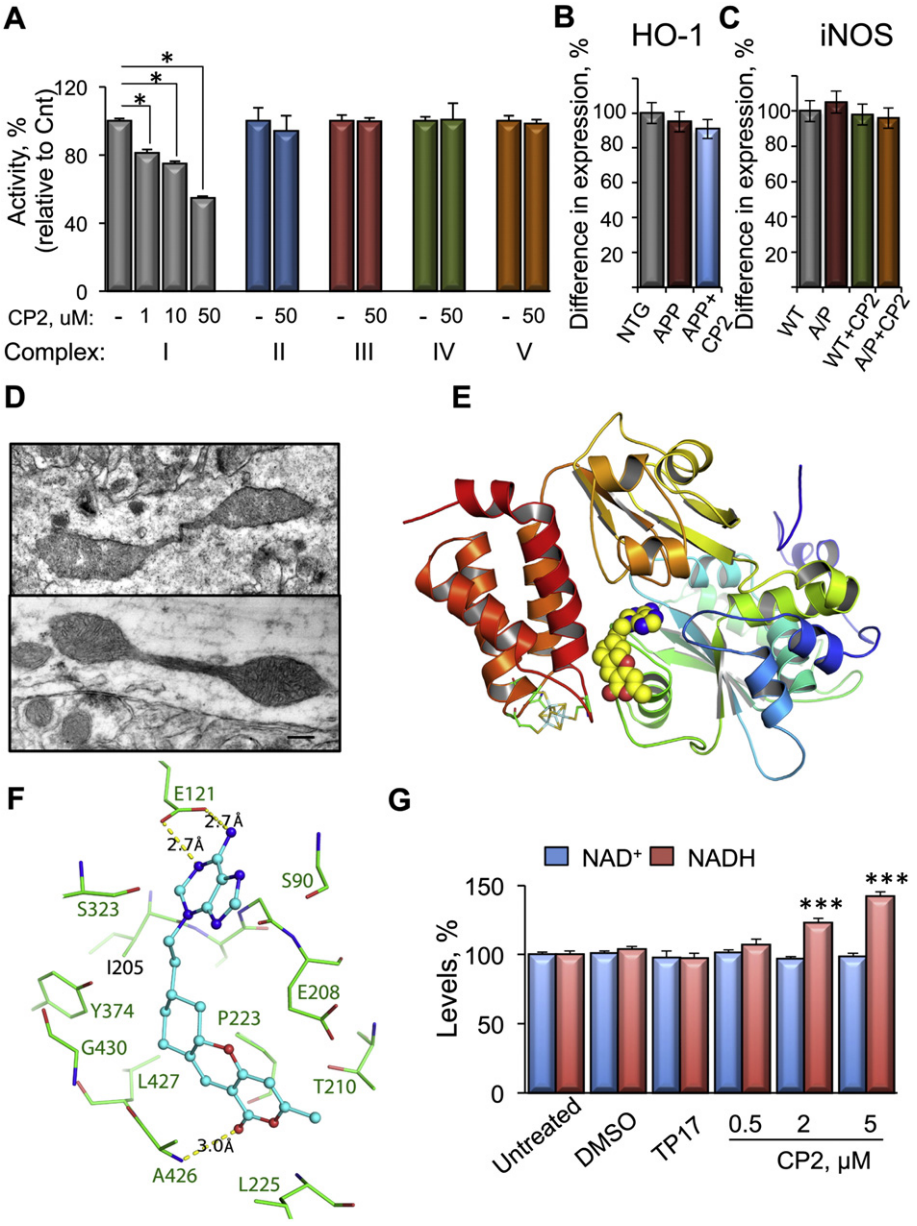

Fig. 5. CP2 binds to the flavin mononucleotide subunit of complex I and inhibits its activity without inducing oxidative stress. (A) Activity of respiratory complexes I–V in isolated mitochondria treated with different concentrations of CP2. $^{*}P < 0.001$, two-tailed *t*-test; n = 3–5 replicates per data point. (B, C) CP2 treatment in APP (25 mg/kg/day, 14 months, n = 4) and APP/PS1 (25 mg/kg/day, 4 months, n = 5) mice did not change the expression of HO-1 (B) and iNOS (C) genes compared to untreated NTG (n = 4) or WT mice (n = 5). (D) Electron micrographs of mitochondria in the hippocampus of APP mouse treated with CP2 for 14 months (bottom) compared to untreated APP mouse (top) of the same age. Scale bar, 500 nm (top) and 200 nm (bottom). (E) Overview of the CP2-bound flavin mononucleotide subunit of human complex I. (F) Residues of the complex I subunit that interact with CP2 (the subunit is in stick model; CP2 is in ball-and-stick model; dashed lines denote hydrogen bonds). (G) Levels of NADH and NAD^{+} in WT neurons treated with different concentration of CP2, vehicle or inactive CP2 analog, TP17; n = 8–11 replicates per data point. $^{***}P < 0.00001$. See also Fig. S6.

of complex IV is predominantly linked to Aβ pathology (Chaturvedi and Flint Beal, 2013), reducing workload through ETC by mild inhibition of complex I could also provide some relief for complex IV. While the detailed correlation between the extent of deficiencies in various ETC complexes and efficacy of CP2 treatment remains to be determined, our pilot data demonstrate that CP2 treatment is efficient in slowing down the development of AD when administered for 6 months to symptomatic APP/PS1 mice starting at 9 months of age (data not shown).

Another important finding of our study is that mild inhibition of complex I resulted in restoration of axonal trafficking. Remarkably, reduction in GSK3β activity, Aβ and pTau was sufficient to restore mitochondrial motility even under conditions where ATP production was slightly reduced. Increased levels of BDNF and synaptic proteins support the notion that trafficking restoration contributes to cognitive protection observed in APP/PS1 mice. These data demonstrates therapeutic value of trafficking restoration in respect to cognitive protection. We previously demonstrated that CP2 binds Aβ preventing its aggregation (Maezawa et al., 2006; Rana et al., 2009). However, it remains to be determined to what extent that contributes to therapeutic efficacy observed in the study. While we detected a reduction in Aβ levels, future investigations are needed to establish whether CP2 affects APP processing, Aβ production and/or enhances autophagic clearance via AMPK-dependent inhibition of the mammalian target of rapamycin.

Our data support a counterintuitive therapeutic approach that is based on the inhibition of OXPHOS. However, emerging data demonstrate that the presence of mtDNA mutations encoding subunits of

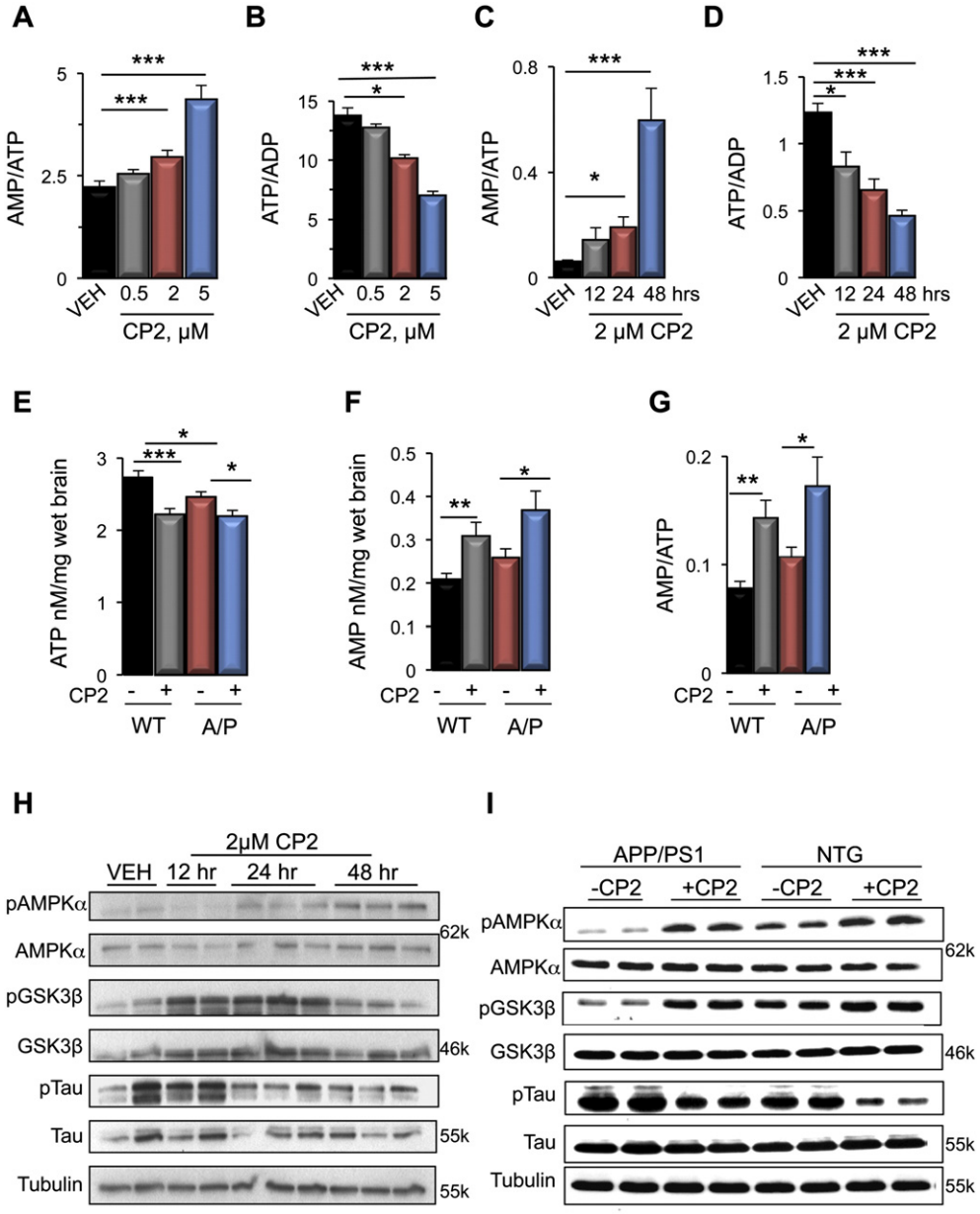

Fig. 6. CP2 treatment increases AMP/ATP ratio and activates AMPK in vitro and in vivo. (A, B) Dose-dependent increase in AMP/ATP (A) and a decrease in ATP/ADP (B) in WT neurons 24 h after CP2 treatment. $^{*}P < 0.05$; $^{***}P < 0.001$; n = 6. (C, D) Time-dependent AMP/ATP increase (C) and ATP/ADP decrease (D) in WT cortical neurons after CP2 treatment. $^{*}P < 0.05$; $^{***}P < 0.001$; n = 6; VEH — vehicle-treated neurons. Data represent mean ± SEM. (E–G) CP2 (25 mg/kg/day, 2 months) reduces ATP levels in the brain of WT (n = 16) and APP/PS1 (A/P, n = 11) mice (E), and increases levels of AMP (F) and AMP/ATP ratio (G). $^{*}P < 0.05$; $^{**}P < 0.01$; $^{***}P < 0.001$. (H) CP2 affects levels of pAMPK, pGSK3β (S9), and pTau (S396) in a time-dependent manner in cortical neurons (P1) from APP/PS1 mice. Each lane represents neurons from individual APP/PS1 animal. (I) CP2 (25 mg/kg/day, 2 months) activates AMPK, reduces activity of GSK3β, and decreases levels of pTau (S396) in the brain of APP/PS1 mice. See also Fig. S7.

complex I or inhibition of OXPHOS with pharmacological inhibitors is beneficial in preventing obesity and type II diabetes (Pospisilik et al., 2007; Quintens et al., 2013; Vernochet et al., 2012; Wredenberg et al., 2006), and promoting longevity in model organisms and in humans (Copeland et al., 2009; Lee et al., 2003; Liu et al., 2005; Raule et al., 2014). Activation of AMPK also underlies molecular mechanisms of metabolic reprogramming induced by calorie restriction (Martin-Montalvo and de Cabo, 2013). While we did not detect significant changes in levels of Sirtuin 1 or peroxisome proliferator-activated receptor gamma coactivator 1 alpha after prolonged treatment with CP2 (data not shown), animals maintained healthy body weight, displayed robust performance in motor tests, and were conceiving longer compared to untreated mice. It will be important to further investigate the molecular mechanisms associated with cognitive protection observed in our study and to determine whether metabolic reprogramming induced by this complex I inhibitor could promote an increase in health and life span.

Supplementary data to this article can be found online at http://dx.doi.org/10.1016/j.ebiom.2015.03.009.

Author Contributions

E.T. conceptualized and supervised the study, and wrote the manuscript; P.D., S.Z., and E.N. measured AMP–ADP; E.T., P.M., and B.G. examined axonal transport; I.M., L.-W.J., Y.Y., T.K., and G.B. quantified Aβ; KO.C. and K.N. performed gene expression; K.P. and T.D.T.N. synthesized/quantified CP2 and amyloid plaques; D.H.H. designed and provided CP2 and analyzed data; Y.-P.P. designed and conducted the computational study. All authors participated in manuscript revisions.

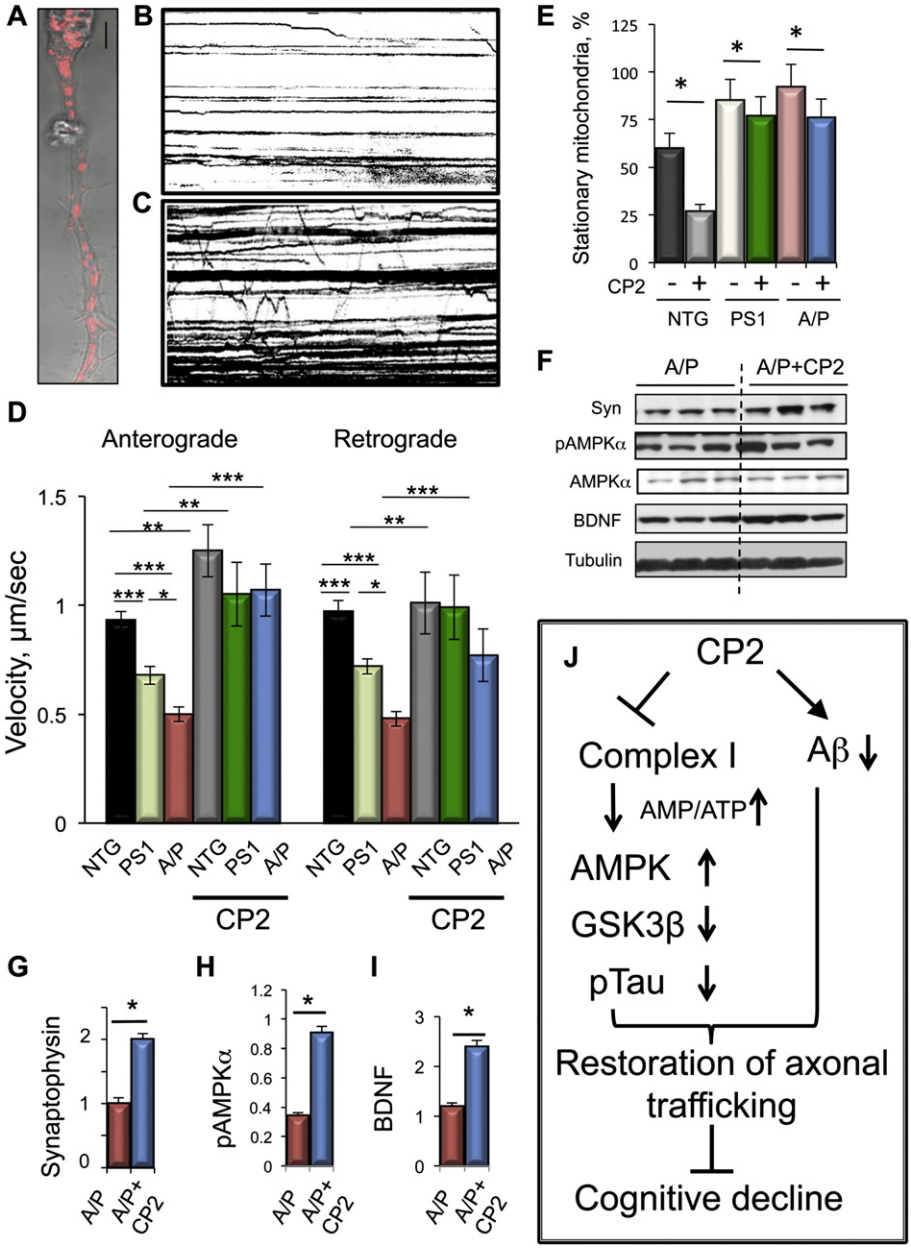

Fig. 7. CP2 restores axonal trafficking and increases levels of synaptic markers and BDNF. (A) Visualization of mitochondria in live neuron using TMRM and LSM 510 confocal microscope, 100× oil DIC lens (1.4 NA). Scale bar, 10 mm. (B, C) Representative kymographs showing reduced axonal transport with primarily stationary mitochondria (horizontal lines) in APP/PS1 neurons (B) and significantly greater mitochondrial motility (diagonal lines) in neurons from APP/PS1 mice treated with CP2 in utero (C). Neurons were plated from P1 animals and imaged after 7 DIC. Data analysis for these experiments is presented in D and E. (D) CP2 restores mitochondrial trafficking in anterograde and retrograde directions in neurons from APP/PS1 (A/P, n = 5) and PS1 (n = 5) P1 pups born from the CP2-treated F2 mice. (E) Mitochondria in neurons from newborn mice treaded with CP2 in utero moved more frequently. All values are presented as mean ± standard error. $^{*}P < 0.05$; $^{**}P < 0.01$; $^{***}P < 0.001$. (F) Western blotting in brain extracts from APP/PS1 (n = 3) mice treated with CP2 (25 mg/kg/day, 2 months) shows an increase in synaptophysin, BDNF and pAMPK compared to untreated APP/PS1 animals (n = 3). (G–I) Fold differences in protein levels from (F) normalized to tubulin using densitometry. $^{*}P < 0.05$. (J) Data interpretation.

Competing Financial Interests

The authors declare no competing financial interests.

Acknowledgments

We thank Mr. K. Howell and K. Johnson for help with animals, Mr. L. Charalambous for generating kymographs, and Mr. T. Christensen for help with EM. This research was supported by grants from NIEHS R01ES020715, ADDF 291204, BrightFocus A2011084, Mayo Clinic ADRC, (Gift from the Gerald and Henrietta Rauenhorst Foundation) NCATS UL1 TR000135 (all to E.T.), and NIH AG025500 and P30 AG10129 (D.H.H., L.-W.J.). Its contents are solely the responsibility of the authors and do not necessarily represent the official views of the NIH. Funding sources did not have any involvement in study design or data analysis and interpretation.

References

Braak, H., Braak, E., 1991. Neuropathological stageing of Alzheimer-related changes. Acta Neuropathol. 82, 239–259.
Cai, Z., Yan, L.J., Li, K., Quazi, S.H., Zhao, B., 2012. Roles of AMP-activated protein kinase in Alzheimer's disease. Neuromolecular Med. 14, 1–14.
Chaturvedi, R.K., Flint Beal, M., 2013. Mitochondrial diseases of the brain. Free Radic. Biol. Med. 63, 1–29.

Choi, S.W., Gerencser, A.A., Nicholls, D.G., 2009. Bioenergetic analysis of isolated cerebrocortical nerve terminals on a microgram scale: spare respiratory capacity and stochastic mitochondrial failure. J. Neurochem. 109, 1179–1191.

Copeland, J.M., Cho, J., Lo Jr., T., Hur, J.H., Bahadorani, S., Arabyan, T., Rabie, J., Soh, J., Walker, D.W., 2009. Extension of *Drosophila* life span by RNAi of the mitochondrial respiratory chain. Curr. Biol. 19, 1591–1598.

Cummings, J.L., Morstorf, T., Zhong, K., 2014. Alzheimer's disease drug-development pipeline: few candidates, frequent failures. Alzheimers Res. Ther. 6, 37.

Darrouzet, E., Issartel, J.P., Lunardi, J., Dupuis, A., 1998. The 49-kDa subunit of NADH-ubiquinone oxidoreductase (Complex I) is involved in the binding of piericidin and rotenone, two quinone-related inhibitors. FEBS Lett. 431, 34–38.

Dumont, M., Beal, M.F., 2011. Neuroprotective strategies involving ROS in Alzheimer disease. Free Radic. Biol. Med. 51, 1014–1026.

Gupta, A., Bisht, B., Dey, C.S., 2011. Peripheral insulin-sensitizer drug metformin ameliorates neuronal insulin resistance and Alzheimer's-like changes. Neuropharmacology 60, 910–920.

Hardie, D.G., 2007. AMP-activated/SNF1 protein kinases: conserved guardians of cellular energy. Nat. Rev. Mol. Cell Biol. 8, 774–785.

Hirst, J., Carroll, J., Fearnley, I.M., Shannon, R.J., Walker, J.E., 2003. The nuclear encoded subunits of complex I from bovine heart mitochondria. Biochim. Biophys. Acta 1604, 135–150.

Hirst, J., King, M.S., Pryde, K.R., 2008. The production of reactive oxygen species by complex I. Biochem. Soc. Trans. 36, 976–980.

Holcomb, L., Gordon, M.N., McGowan, E., Yu, X., Benkovic, S., Jantzen, P., Wright, K., Saad, I., Mueller, R., Morgan, D., et al., 1998. Accelerated Alzheimer-type phenotype in transgenic mice carrying both mutant amyloid precursor protein and presenilin 1 transgenes. Nat. Med. 4, 97–100.

Holtzman, D.M., Morris, J.C., Goate, A.M., 2011. Alzheimer's disease: the challenge of the second century. Sci. Transl. Med. 3, 77sr71.

Hong, H.S., Rana, S., Barrigan, L., Shi, A., Zhang, Y., Zhou, F., Jin, L.W., Hua, D.H., 2009. Inhibition of Alzheimer's amyloid toxicity with a tricyclic pyrone molecule in vitro and in vivo. J. Neurochem. 108, 1097–1108.

Horike, N., Sakoda, H., Kushiyama, A., Ono, H., Fujishiro, M., Kamata, H., Nishiyama, K., Uchijima, Y., Kurihara, Y., Kurihara, H., et al., 2008. AMP-activated protein kinase activation increases phosphorylation of glycogen synthase kinase 3beta and thereby reduces cAMP-responsive element transcriptional activity and phosphoenolpyruvate carboxykinase C gene expression in the liver. J. Biol. Chem. 283, 33902–33910.

Hua, D.H., Chen, Y., Sin, H.-S., Maroto, M.J., Robinson, P.D., Newell, S.W., Perchellet, E.M., Ladesich, J.B., Freeman, J.A., Perchellet, J.-P., et al., 1997. A one-pot condensation of pyrones and enals. Synthesis of 1H,7H-5a,6,8,9-tetrahydro-1-oxopyrano[4,3-b][1]benzopyrans. J. Org. Chem. 62, 6888–6896.

Hua, D.H., Huang, X., Tamura, M., Chen, Y., Woltkamp, M., Jin, L., Perchellet, E.M., Perchellet, J., Chiang, P.K., Namatame, I., et al., 2003. Syntheses and bioactivities of tricyclic pyrones. Tetrahedron 4795–4803.

Imfeld, P., Bodmer, M., Jick, S.S., Meier, C.R., 2012. Metformin, other antidiabetic drugs, and risk of Alzheimer's disease: a population-based case–control study. J. Am. Geriatr. Soc. 60, 916–921.

Jack Jr., C.R., Holtzman, D.M., 2013. Biomarker modeling of Alzheimer's disease. Neuron 80, 1347–1358.

Kanekiyo, T., Cirrito, J.R., Liu, C.C., Shinohara, M., Li, J., Schuler, D.R., Holtzman, D.M., Bu, G., 2013. Neuronal clearance of amyloid-beta by endocytic receptor LRP1. J. Neurosci. 33, 19276–19283.

Kenyon, C.J., 2010. The genetics of ageing. Nature 464, 504–512.

Kickstein, E., Krauss, S., Thornhill, P., Rutschow, D., Zeller, R., Sharkey, J., Williamson, R., Fuchs, M., Kohler, A., Glossmann, H., et al., 2010. Biguanide metformin acts on tau phosphorylation via mTOR/protein phosphatase 2A (PP2A) signaling. Proc. Natl. Acad. Sci. U. S. A. 107, 21830–21835.

King, M.S., Sharpley, M.S., Hirst, J., 2009. Reduction of hydrophilic ubiquinones by the flavin in mitochondrial NADH:ubiquinone oxidoreductase (Complex I) and production of reactive oxygen species. Biochemistry 48, 2053–2062.

Lee, S.S., Lee, R.Y., Fraser, A.G., Kamath, R.S., Ahringer, J., Ruvkun, G., 2003. A systematic RNAi screen identifies a critical role for mitochondria in *C. elegans* longevity. Nat. Genet. 33, 40–48.

Liu, X., Jiang, N., Hughes, B., Bigras, E., Shoubridge, E., Hekimi, S., 2005. Evolutionary conservation of the clk-1-dependent mechanism of longevity: loss of mclk1 increases cellular fitness and lifespan in mice. Genes Dev. 19, 2424–2434.

Maezawa, I., Jin, L.W., Woltjer, R.L., Maeda, N., Martin, G.M., Montine, T.J., Montine, K.S., 2004. Apolipoprotein E isoforms and apolipoprotein AI protect from amyloid precursor protein carboxy terminal fragment-associated cytotoxicity. J. Neurochem. 91, 1312–1321.

Maezawa, I., Hong, H.S., Wu, H.C., Battina, S.K., Rana, S., Iwamoto, T., Radke, G.A., Pettersson, E., Martin, G.M., Hua, D.H., et al., 2006. A novel tricyclic pyrone compound ameliorates cell death associated with intracellular amyloid-beta oligomeric complexes. J. Neurochem. 98, 57–67.

Mair, W., Morantte, I., Rodrigues, A.P., Manning, G., Montminy, M., Shaw, R.J., Dillin, A., 2011. Lifespan extension induced by AMPK and calcineurin is mediated by CRTC-1 and CREB. Nature 470, 404–408.

Mairet-Coello, G., Courchet, J., Pieraut, S., Courchet, V., Maximov, A., Polleux, F., 2013. The CAMKK2–AMPK kinase pathway mediates the synaptotoxic effects of Abeta oligomers through tau phosphorylation. Neuron 78, 94–108.

Martin-Montalvo, A., de Cabo, R., 2013. Mitochondrial metabolic reprogramming induced by calorie restriction. Antioxid. Redox Signal. 19, 310–320.

Mondragon-Rodriguez, S., Perry, G., Zhu, X., Boehm, J., 2012. Amyloid beta and tau proteins as therapeutic targets for Alzheimer's disease treatment: rethinking the current strategy. Int. J. Alzheimers Dis. 2012, 630182.

Moore, E.M., Mander, A.G., Ames, D., Kotowicz, M.A., Carne, R.P., Brodaty, H., Woodward, M., Boundy, K., Ellis, K.A., Bush, A.I., et al., 2013. Increased risk of cognitive impairment in patients with diabetes is associated with metformin. Diabetes Care 36, 2981–2987.

Nath, K.A., Grande, J.P., Haggard, J.J., Croatt, A.J., Katusic, Z.S., Solovey, A., Hebbel, R.P., 2001. Oxidative stress and induction of heme oxygenase-1 in the kidney in sickle cell disease. Am. J. Pathol. 158, 893–903.

Okado-Matsumoto, A., Fridovich, I., 2001. Subcellular distribution of superoxide dismutases (SOD) in rat liver: Cu,Zn-SOD in mitochondria. J. Biol. Chem. 276, 38388–38393.

Omura, S., Tomoda, H., Kim, Y.K., Nishida, H., 1993. Pyripyropenes, highly potent inhibitors of acyl-CoA:cholesterol acyltransferase produced by *Aspergillus fumigatus*. J. Antibiot. 46, 1168–1169.

Omura, S., Kuno, F., Otoguro, K., Sunazuka, T., Shiomi, K., Masuma, R., Iwai, Y., 1995. Arisugacin, a novel and selective inhibitor of acetylcholinesterase from *Penicillium* sp. FO-4259. J. Antibiot. 48, 745–746.

Orth, M., Schapira, A.H., 2001. Mitochondria and degenerative disorders. Am. J. Med. Genet. 106, 27–36.

Pang, Y.P., 2014. Low-mass molecular dynamics simulation: a simple and generic technique to enhance configurational sampling. Biochem. Biophys. Res. Commun. 452, 588–592.

Parihar, M.S., Brewer, G.J., 2007. Mitoenergetic failure in Alzheimer disease. Am. J. Physiol. Cell Physiol. 292, C8–C23.

Park, H., Kam, T.I., Kim, Y., Choi, H., Gwon, Y., Kim, C., Koh, J.Y., Jung, Y.K., 2012. Neuropathogenic role of adenylate kinase-1 in Abeta-mediated tau phosphorylation via AMPK and GSK3beta. Hum. Mol. Genet. 21, 2725–2737.

Peralta, S., Torraco, A., Wenz, T., Garcia, S., Diaz, F., Moraes, C.T., 2014. Partial complex I deficiency due to the CNS conditional ablation of Ndufa5 results in a mild chronic encephalopathy but no increase in oxidative damage. Hum. Mol. Genet. 23, 1399–1412.

Pernicova, I., Korbonits, M., 2014. Metformin — mode of action and clinical implications for diabetes and cancer. Nat. Rev. Endocrinol. 10, 143–156.

Pimplikar, S.W., Nixon, R.A., Robakis, N.K., Shen, J., Tsai, L.H., 2010. Amyloid-independent mechanisms in Alzheimer's disease pathogenesis. J. Neurosci. 30, 14946–14954.

Pokhrel, L., Maezawa, I., Nguyen, T.D., Chang, K.O., Jin, L.W., Hua, D.H., 2012. Inhibition of Acyl-CoA:cholesterol acyltransferase (ACAT), overexpression of cholesterol transporter gene, and protection of amyloid beta (Abeta) oligomers-induced neuronal cell death by tricyclic pyrone molecules. J. Med. Chem. 55, 8969–8973.

Poon, W.W., Blurton-Jones, M., Tu, C.H., Feinberg, L.M., Chabrier, M.A., Harris, J.W., Jeon, N.L., Cotman, C.W., 2011. Beta-amyloid impairs axonal BDNF retrograde trafficking. Neurobiol. Aging 32, 821–833.

Porquet, D., Casadesus, G., Bayod, S., Vicente, A., Canudas, A.M., Vilaplana, J., Pelegri, C., Sanfeliu, C., Camins, A., Pallas, M., et al., 2013. Dietary resveratrol prevents Alzheimer's markers and increases life span in SAMP8. Age 35, 1851–1865.

Pospisilik, J.A., Knauf, C., Joza, N., Benit, P., Orthofer, M., Cani, P.D., Ebersberger, I., Nakashima, T., Sarao, R., Neely, G., et al., 2007. Targeted deletion of AIF decreases mitochondrial oxidative phosphorylation and protects from obesity and diabetes. Cell 131, 476–491.

Profenno, L.A., Porsteinsson, A.P., Faraone, S.V., 2010. Meta-analysis of Alzheimer's disease risk with obesity, diabetes, and related disorders. Biol. Psychiatry 67, 505–512.

Quintens, R., Singh, S., Lemaire, K., De Bock, K., Granvik, M., Schraenen, A., Vroegrijk, I.O., Costa, V., Van Noten, P., Lambrechts, D., et al., 2013. Mice deficient in the respiratory chain gene Cox6a2 are protected against high-fat diet-induced obesity and insulin resistance. PLoS One 8, e56719.

Rana, S., Hong, H.S., Barrigan, L., Jin, L.W., Hua, D.H., 2009. Syntheses of tricyclic pyrones and pyridinones and protection of Abeta-peptide induced MC65 neuronal cell death. Bioorg. Med. Chem. Lett. 19, 670–674.

Raule, N., Sevini, F., Li, S., Barbieri, A., Tallaro, F., Lomartire, L., Vianello, D., Montesanto, A., Moilanen, J.S., Bezrukov, V., et al., 2014. The co-occurrence of mtDNA mutations on different oxidative phosphorylation subunits, not detected by haplogroup analysis, affects human longevity and is population specific. Aging Cell 13, 401–407.

Salminen, A., Kaarniranta, K., 2012. AMP-activated protein kinase (AMPK) controls the aging process via an integrated signaling network. Ageing Res. Rev. 11, 230–241.

Salminen, A., Kaarniranta, K., Haapasalo, A., Soininen, H., Hiltunen, M., 2011. AMP-activated protein kinase: a potential player in Alzheimer's disease. J. Neurochem. 118, 460–474.

Shirwany, N.A., Zou, M.H., 2014. AMPK: a cellular metabolic and redox sensor. A minireview. Front. Biosci. (Landmark Ed.) 19, 447–474.

Spinazzi, M., Casarin, A., Pertegato, V., Salviati, L., Angelini, C., 2012. Assessment of mitochondrial respiratory chain enzymatic activities on tissues and cultured cells. Nat. Protoc. 7, 1235–1246.

Thies, W., Bleiler, L., Association, A.S., 2013. 2013 Alzheimer's disease facts and figures. Alzheimers Dement. 9, 208–245.

Trushina, E., Dyer, R.B., Badger II, J.D., Ure, D., Eide, L., Tran, D.D., Vrieze, B.T., Legendre-Guillemin, V., McPherson, P.S., Mandavilli, B.S., et al., 2004. Mutant huntingtin impairs axonal trafficking in mammalian neurons in vivo and in vitro. Mol. Cell. Biol. 24, 8195–8209.

Trushina, E., Nemutlu, E., Zhang, S., Christensen, T., Camp, J., Mesa, J., Siddiqui, A., Tamura, Y., Sesaki, H., Wengenack, T.M., et al., 2012. Defects in mitochondrial dynamics and metabolomic signatures of evolving energetic stress in mouse models of familial Alzheimer's disease. PLoS One 7.

Vernochet, C., Mourier, A., Bezy, O., Macotela, Y., Boucher, J., Rardin, M.J., An, D., Lee, K.Y., Ilkayeva, O.R., Zingaretti, C.M., et al., 2012. Adipose-specific deletion of TFAM increases mitochondrial oxidation and protects mice against obesity and insulin resistance. Cell Metab. 16, 765–776.

Vicario-Orri, E., Opazo, C.M., Munoz, F.J., 2015. The pathophysiology of axonal transport in Alzheimer's disease. J. Alzheimers Dis. 43, 1097–1113.

Vingtdeux, V., Giliberto, L., Zhao, H., Chandakkar, P., Wu, Q., Simon, J.E., Janle, E.M., Lobo, J., Ferruzzi, M.G., Davies, P., et al., 2010. AMP-activated protein kinase signaling activation by resveratrol modulates amyloid-beta peptide metabolism. J. Biol. Chem. 285, 9100–9113.

Vingtdeux, V., Chandakkar, P., Zhao, H., d'Abramo, C., Davies, P., Marambaud, P., 2011. Novel synthetic small-molecule activators of AMPK as enhancers of autophagy and amyloid-beta peptide degradation. FASEB J. 25, 219–231.

Wredenberg, A., Freyer, C., Sandstrom, M.E., Katz, A., Wibom, R., Westerblad, H., Larsson, N.G., 2006. Respiratory chain dysfunction in skeletal muscle does not cause insulin resistance. Biochem. Biophys. Res. Commun. 350, 202–207.

Wu, M., Neilson, A., Swift, A.L., Moran, R., Tamagnine, J., Parslow, D., Armistead, S., Lemire, K., Orrell, J., Teich, J., et al., 2007. Multiparameter metabolic analysis reveals a close link between attenuated mitochondrial bioenergetic function and enhanced glycolysis dependency in human tumor cells. Am. J. Physiol. Cell Physiol. 292, C125–C136.